

---

# LIGHT FIELD COMPRESSION BY RESIDUAL CNN ASSISTED JPEG

---

A PREPRINT

**Eisa Hedayati**  
Michigan Technological University  
hedayati@mtu.edu

**Timothy C. Havens**  
Michigan Technological University  
thavens@mtu.edu

**Jeremy P. Bos**  
Michigan Technological University  
jpbos@mtu.edu

March 15, 2022

## ABSTRACT

Light field (LF) imaging has gained significant attention due to its recent success in 3-dimensional (3D) displaying and rendering as well as augmented and virtual reality usage. Nonetheless, because of the two extra dimensions, LFs are much larger than conventional images. We develop a JPEG-assisted learning-based technique to reconstruct an LF from a JPEG bitstream with a bit per pixel ratio of 0.0047 on average. For compression, we keep the LF’s center view and use JPEG compression with 50% quality. Our reconstruction pipeline consists of a small JPEG enhancement network (JPEG-Hance), a depth estimation network (Depth-Net), followed by view synthesizing by warping the enhanced center view. Our pipeline is significantly faster than using video compression on pseudo-sequences extracted from an LF, both in compression and decompression, while maintaining effective performance. We show that with a 1% compression time cost and 18x speedup for decompression, our methods reconstructed LFs have better structural similarity index metric (SSIM) and comparable peak signal-to-noise ratio (PSNR) compared to the state-of-the-art video compression techniques used to compress LFs.

## 1 Introduction(to be completed based on the length)

*Light fields* (LF) have two extra dimensions, as compared to conventional images, which represents angular information of the scene. Hence, LFs contain a large volume of data that makes storing and portability time consuming and costly. Also, decompressing LF video with a high angular resolution at acceptable *frames per second*(fps) for streaming is challenging. We aim to address these problems by predicting the entire LF from its JPEG compressed center view.

Direct application of the standard image compression techniques, such as JPEG, PNG, *etc*let@tokeneonedot, on the LF do not take advantage of the existing redundancy between LF views. A better success has been achieved from the use of video compression techniques. For using video compression methods on LFs, a sequence of images has been build from LF views which is called pseudo-sequence[1]. A combination of machine learning (ML) methods, capable of predicting LF views, and video compression techniques, has been explored in [2]. In this work, we present a combination of JPEG compression with ML view predictions. LF synthesis techniques have shown the possibility of estimating the entire LF from a single or a set of sparse views. Here, we show that there is enough information in the JPEG compressed center view—as well as a group of sub-aperture images (SAI)—to predict the entire LF with sufficient quality. We test the success of our method by comparing against state-of-the-art methods in LF compression that use the existing HEVC compression.

Our method is faster in compression and decompression by 100x and 10x, respectively, compared to the direct use of HEVC. This speed up means a set of 30 LFs with a spatial resolution of (375, 540) and angular resolution of (7, 7) can be decompressed on a typical gaming GPU in less than 0.02 second, while HEVC-based methods it takes more than 0.39 second. We can see that a little increase in spatial or angular dimensions will kick HEVC-based methods out of 1 second easily. Thus, streaming with not be possible. While speeding up the process, we have maintained and, in most cases, improved the quality of reconstruction at the same *bit per pixel* (bpp) ratio. We have used the *mean of peak signal-to-noise* (MPSNR) ratio over all of the views and *mean structural similarity index metric* (MSSIM) to

compare the reconstructed LFs of our model with those that use HEVC. We show that while the MPSNR of our method is comparable to the direct employment of HEVC, our model can achieve higher MSSIM. This results in fewer artifacts and better quality in the extracted synthetic aperture *depth of field* (DoF) images.

The contributions of this paper are as follows: We achieved compression speed up of more than 100x, and decompression speed up of more than 10x compared to use of HEVC on pseudo-sequence of LF views. At average bpp of .0047 the LF's DoF reconstructed with our method improved the SSIM by .31% on average compared to the direct use of HEVC. Finally, we introduce a small, fast and efficient *convolutional neural network* (CNN) for enhancing JPEG images. This network also boosts the SSIM of the final decompressed LF.

## 2 Related Work

### 2.1 Light Field View Synthesis

Linear view synthesis by Levin and Durand [3] and depth of field extension and super-resolution by Bishop and Favaro [4] are among the earliest works on LF view synthesis and reconstruction. Flynn *et allet@tokeneonedot*[5] proposed a deep learning method to predict novel views from a sequence of images with wide baselines. LF view synthesis became more popular after Kalantari *et allet@tokeneonedot*[6] showed in their work that an LF can be synthesized from its corner SAIs with high quality. Building on the work of Kalantari *et allet@tokeneonedot*, Yeung *et allet@tokeneonedot* used different sets of views to reconstruct dense LFs [7]. Srinivasan *et allet@tokeneonedot* demonstrate the possibility of estimating the entire LF from its center view by extrapolating using machine learning methods [8]. Choi *et allet@tokeneonedot* extended the extrapolation to an LF taken with arrays of cameras [9]. LF fusion [10] and Depth-guided techniques [11] have been popular in reconstructing an LF from a single or a sparse set of SAIs. Hu *et allet@tokeneonedot*[12] aimed for a faster LF reconstruction method by using hierarchical features fusion.

The backbone of nearly every view synthesis method enumerated here is the depth-map estimation. the current work is categorized as single view LF reconstruction. Our method is unique because we use a lossy compressed JPEG view from which to estimate the entire LF. We use residual learning methods to guess the possible artifacts from the JPEG compressed version of the center view to assist the main network for accurately estimating the depth map.

### 2.2 Light Field Compression

Lossless and lossy compression methods have been investigated extensively in the literature. For the lossless model, Perra [13] proposed an adaptive block differential prediction method and Helin *et allet@tokeneonedot*[14] described a sparse modeling with a predictive coding for SAIs of the LF.

The lossy models can be classified in to sub-categories of: standardized image/video compression techniques and machine learning assisted compression techniques.

#### 2.2.1 LF compression by standardized image/video compression methods

Standardized image and video compression techniques (especially HEVC) have been directly used to address the problem of the bulkiness of LF, see e.g., [1, 15, 16]. Other methods, such as homography-based low-rank models [17] and Fourier Disparity Layers [18], have been used to reduce the angular dimension of the LF. In another work, the LF depth was segmented into 4D spatial-angular blocks, which was used for prediction, followed by encoding the residue using JPEG-2000 [19].

#### 2.2.2 Machine learning assisted compression techniques

Followed by the breakthrough in synthesizing LF views from its four corners using CNN learning techniques introduced by [6], another work introduced a compression technique by using the same method and compressing the four corner views by HEVC [20]. In another work, the authors proposed to keep half of the views and encode them by HEVC and synthesize the other half by a CNN [2]. A CNN based epipolar plane image super-resolution algorithm was used in cooperation with HEVC to compress LF as well [21]. Wang *et allet@tokeneonedot* proposed a new LF video compression technique by deploying view synthesis methods from multiple inputs while encoding the input views by a proposed region-of-interest scheme [22].

To the best of our knowledge, because the view extrapolation is ill posed, LF reconstruction from a lossy compressed single input (specifically, JPEG) has not been explored before our work.

### 2.3 JPEG Compression Artifact Reduction

For several decades, different researchers addressed the JPEG compression artifact reduction generally in three main groups: prior knowledge-based, filter-based, and learning-based approaches. Here though, we are interested in the learning-based approaches. The basic intention of the learning-based methods is to find a non-linear mapping between the JPEG compressed image—compressed at different compression ratios—to the ground truth uncompressed image. To the best of our knowledge, the first deep learning model to address this problem was created by Dong *et al* [23], where they showed the possibility of enhancing the reconstructed JPEG image by a relatively shallow CNN. Since then, multiple researchers have gradually improved the performance of learning-based methods by introducing new networks such as: dual-domain representations [24], deep dual-domain based fast restoration [25], encoder-decoder networks with symmetric skip connection [26], CAS-CNN [27], one-to-one networks [28], DMCNN [29], and dual-stream multi-path recursive Residual Network [30]. While deeper networks and state of the art architectures have improved the task of JPEG artifact reduction, we are not focused solely on this task here. The ultimate goal of our JPEG-Hance network is to improve the estimated depth-map from the JPEG compressed center image of an LF. JPEG artifact reduction is the natural first step for extracting better depth-maps.

## 3 The Proposed Method

Here we describe our compression and decompression pipeline. The compression pipeline is simply extraction of the center view of the LF, compression by JPEG at 50% quality, followed by discarding of all other views. The decompression pipeline has the following steps:

1. JPEG decompression of the center view  $c_J$

2. Enhancing  $c_J$  by JPEG-Hance to  $c_E$ ,

$$c_E = J(c_J). \quad (1)$$

3. Estimating depth map  $d(x, u)$  of every view  $u$  from  $c_E$ ,

$$d = D(c_E). \quad (2)$$

4. Reconstructing LF by

$$L(x, u)_{u_0 \rightarrow u} = L(x + (u - u_0)d(x, u), u_0), \quad (3)$$

where  $L$  is the approximated LF and  $u_0$  is the middle view index. Variables  $x$  and  $u$  are spatial and angular indices.

### 3.1 Networks architectures

#### 3.1.1 JPEG-Hance

The main goal of our JPEG-Hance network is to assist the Depth-Net in providing better depth map estimation. In doing so, it is certainly beneficial to improve the overall quality of the JPEG decompressed image by reducing the error between uncompressed ground truth images and the lossy compressed ones. However, the goal of our network is not general JPEG artifact reduction; instead, JPEG-Hance should learn to enhance the parts of the image which have the most effect on improving depth information extraction. To achieve this task, JPEG-Hance also needs to find correspondence information from the extracted depth maps. Therefore, it is trained in two phases: first, it learns to enhance any typical JPEG decompressed image, then again as part of the whole depth estimation pipeline. The architecture of JPEG-Hance is shown in Fig. 1. Encouraged by ResNet50’s *bottleneck* building blocks structure, we have designed our JPEG-Hance residual blocks. We have added a *batch normalization* (BN) layer after each convolution followed by an exponential linear unit (ELU). The ELU followed by a last layer *tanh* seems to be the most promising activation pair of functions when dealing with regression of image data scaled to the interval  $[-1, 1]$ .

JPEG-Hance is pre-trained by minimizing the mean squared error of each pixel value in the RGB channels. Then it will be added to the training pipeline for full reconstruction of LFs.

#### 3.1.2 Depth-Net

Multiple images provide geometry information which can be used for LF reconstruction. A single image does not provide such information. Therefore, such information should be extracted by other methods. Machine learning techniques, particularly CNNs showed a promising potential for estimating geometry from a single image [8, 6, 7]. Thus, for the problem of depth estimation from our enhanced center image, we use a residual CNN.

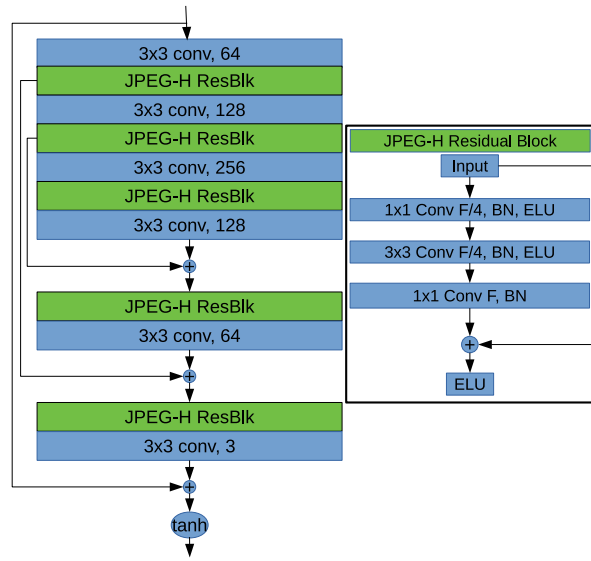


Figure 1: JPEG-Hance detailed structure

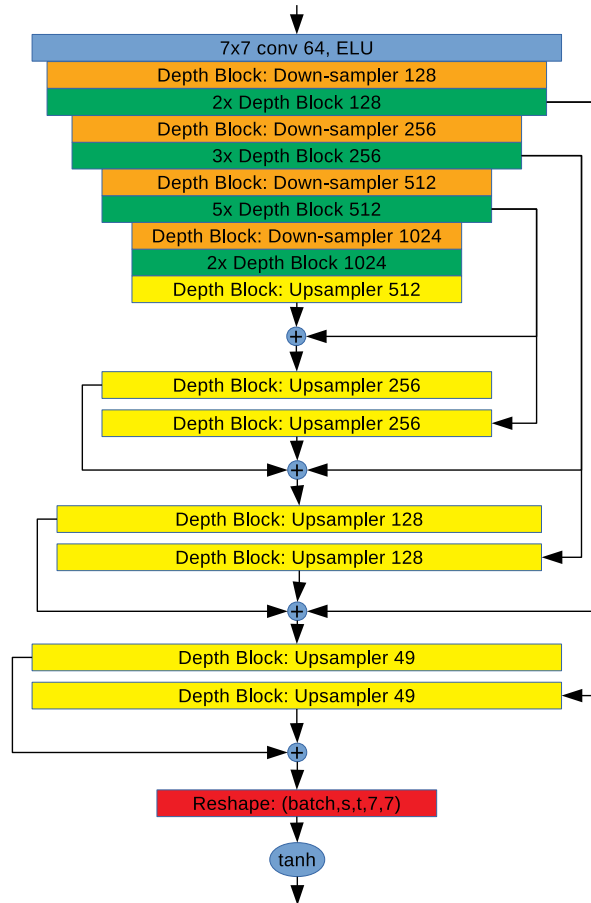


Figure 2: Depth-Net detailed structure

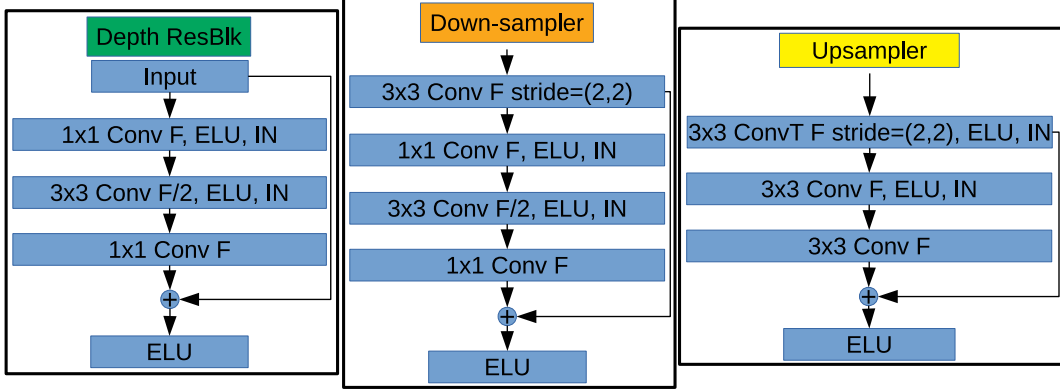


Figure 3: Depth-Net residual blocks

Our Depth-Net is responsible for estimating corresponding depth map (disparity map) for all 49 views from the middle JPEG compressed view. The structure of Depth-Net is depicted in Fig. 2. The Depth net has three variants of residual blocks. The first variant is a down-sampler which uses a 2D convolution with strides of  $(2 \times 2)$ , halving the spatial dimension of the input image. This block is used just before the first Depth Residual Block; each time the feature size is increased. The second type of block, the Depth Residual block, is the main residual block. This block is used the most and extracts most of the features. The structure of the Depth Residual block mimics the bottleneck structure of ResNet50 with added instance normalization after each of the first two convolution layers. Last, the Upsampler block is constructed to have a 2D deconvolution (transposed convolution) layer and two 2D convolution layers with kernel size of  $(3 \times 3)$ . The deconvolution layer’s stride is set to  $(2 \times 2)$ . These blocks are shown in Fig. 3.

Because we are training the Depth-Net on the actual LF data and not the ground truth depth maps, our loss functions have to be designed to train the network in an unsupervised manner. Thus, we define the Depth-Net pre-training loss function to be a weighted sum of four sub-functions: i) photometric loss  $L_p$ , ii) defocus loss  $L_r$ , iii) depth-consistency loss  $L_c$ , and iv) DoF loss  $L_d$ .

$$L_{depth} = \alpha L_p + \alpha_1 L_r + \alpha_2 L_c + \alpha_3 L_d, \quad (4)$$

where  $\alpha, \alpha_1, \alpha_2$  and  $\alpha_3$  are chosen to be 2, 100, 0.02, and 10 in our conducted experiment which are empirically found to work well overall.

The image quality comparison sub-function  $\psi$  [11] is constructed by combining mean absolute difference of pixels and image structural dissimilarity (DSSIM) that is derived from the structural similarity index metric (SSIM) [31]:

$$\psi(I_1, I_2) = \beta \frac{1 - SSIM(I_1, I_2)}{2} + (1 - \beta) \|I_1 - I_2\|_1, \quad (5)$$

where  $I_1, I_2$  are two images that are being compared and  $\beta$  is a number in range  $(0, 1)$ , which we empirically found that 0.15 yields better training results compared to other values. Using the sub-function  $\psi$ , photometric loss is defined to be [11]

$$L_p = \sum_u [\psi(L(x, u)_{u_0 \rightarrow u}, L(x, u)) + \psi(L(x, u)_{u \rightarrow u_0}, L(x, u_0))]. \quad (6)$$

Because we are training an unsupervised Depth-Net, the more prior knowledge we can give the network, the better will be the training quality. Zhou *et allet@tokeneonedot*[11] introduced defocus cue loss to be

$$L_d = \psi(L(x, u_0), \frac{1}{N} \sum_u L(x, u)_{u \rightarrow u_0}). \quad (7)$$

Also depth consistency (left-right or forward-backward) has been shown in the literature [32, 33, 34] to be a promising regularizer for LF view synthesis purpose, where

$$d_{u_0 \rightarrow u}(x) = d_{u_0}(x, (u - u_0)d(x, u)), \quad (8a)$$

$$L_c = \sum_u \|d_u(x) - d_{u_0 \rightarrow u}(x)\|_1. \quad (8b)$$

Finally we have included depth of field (DoF) loss to further assist the network in learning depth information:

$$DoF = \frac{1}{u} \sum_u L(x, u), \quad (9a)$$

$$L_{dof} = \psi(DoF, DoF_{u_0 \rightarrow u}). \quad (9b)$$

## 4 Experiments

In this section, we describe our method’s implementation details. Then, we use public data sets [8, 6] to evaluate our method and investigate the impact of different parts of our network on the performance of our model.

### 4.1 Data sets

We have conducted our experiments over the two public data sets: *Flowers* [8] and *30 Scenes* [6]. Both of these data sets are captured by a Lytro Illum camera. The angular resolution of these data sets is  $14 \times 14$  views and the spatial resolution is variable between  $375 \times 540$  and  $376 \times 541$  pixels.

The LF from these data sets are cropped to the size of  $7 \times 7 \times 375 \times 540$  to have a consistent size and vignetting.

### 4.2 Implementation details

Our pipeline has been trained in multiple steps. The input pipeline was one of the main variables during the training phase.

We have implemented our model with Tensorflow 2.2 in python 3.7 on a workstation with an Intel Xeon W-2223 3.60 GHz, 64GB DDR4 memory, and NVIDIA Quadro RTX 5000.

#### 4.2.1 JPEG-Hance

Our JPEG-Hance has been pre-trained on the *30 Scenes* training data set, which contains 100 scenes. The center views of these 100 scenes are extracted and used for training. In the training phase, the spatial dimensions of the JPEG-Hance are set to  $128 \times 128$ . First a training pool of images with dimensions of  $128 \times 128$  is created by cropping the center views of the 100 scenes at 8 pixels steps. Therefore, the training pool had 150,000 different crops which we found sufficient for the JPEG-Hance network to be trained without over-fitting or under-fitting. The learning rate was set to 0.0004.

The JPEG-Hance has a relatively small network and only has 202,435 trainable parameters. The pre-training phase takes about 90 minutes to converge.

#### 4.2.2 Depth-Net

Our Depth-Net also has a pre-training step. The Depth-Net has been pre-trained on the *Flowers* data set, which has 3,343 flowers. During the pre-training phase, the JPEG-Hance is used for enhancing center images while only Depth-Net parameters are trained. The input pipeline of the flowers contains random croppings to 128 and data augmentation with 50% selection rate for the original data, 15% chance for random contrast change between  $[0.1, 0.5]$ , 15% chance that the brightness is changed randomly up to  $0.4 \times$  original brightness, and the remaining 20% where the hue was randomly changed by up to  $0.4 \times$ . During the pre-training phase, 16 random crops were extracted for each epoch, and the network was trained for 10 epochs. The learning rate was 0.0004.

The Depth-Net is the main network responsible for extracting the depth map, thus, it has more trainable parameters, about 38.2 million. The pre-training phase takes about 7 hours to converge.

#### 4.2.3 Training the entire pipeline

After pre-training the two networks, we now train the entire pipeline, by adding the 100 scenes to the *Flowers* data set pool and using the same input pipeline as the one used for Depth-Net. The entire pipeline has been trained for 45 epochs with gradually decreasing learning rate from 0.0001 to 0.000001 for the last 5 epochs.

The last fine-tuning step includes training the pipeline on the data sets with input spatial dimensions of  $375 \times 540$ . Here the augmentation selection is 25% original, 25% random contrast, 25% random brightness, and 25% random hue. Because of the structure of the Depth-Net network, the input images have to be zero-padded and the resulting LFs

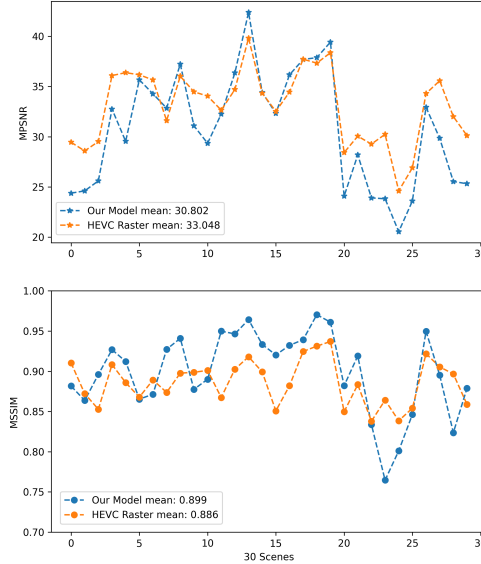


Figure 4: The top figure is showing the MPSNR for each reconstructed LF by our method and HEVC. The bottom figure is the MSSIM calculated for each reconstructed LF.

should be cropped to the correct size. The input dimension of the Depth-Net is  $384 \times 544$ . The fine tuning phase takes 40 epochs for the network to converge with gradually decaying learning rate from 0.00005 to 0.000001. The fine-tuning phase took around 20 hours to converge, while all other pre-training phases took less than 10 hours cumulatively.

### 4.3 Performance comparison

We have compared our compression-decompression results with a pseudo sequence method using the HEVC video compression Codec. We have chosen a raster sequence over spiral because raster had slightly better performance. The 30 scenes data set has been used for comparing our method with HEVC. We use MSSIM and MPSNR metrics as well as SSIM and PSNR of the extracted DoF from LFs to compare the results, where

$$MSSIM = \frac{1}{M} \sum_u SSIM(LF, \tilde{LF}), \quad (10)$$

$$MPSNR = \frac{1}{M} \sum_u PSNR(LF, \tilde{LF}). \quad (11)$$

To have a fair comparison, we have tuned the QP factor of HEVC for each LF to reach approximately similar bpp between HEVC compressed LF and our method’s compressed representative. The average bpp for both methods on the 30 scenes data is 0.0047. We can see in Fig. 4 that the LFs reconstructed by our method have very similar MPSNR and MSSIM to those decompressed by HEVC. By carefully looking at Fig. 4 it will be evident that, while our method is slightly inferior in MPSNR metrics, it outperforms HEVC in MSSIM. Furthermore, in Fig. 5 we can see the calculated PSNR and SSIM metrics for extracted DoFs from the reconstructed LFs. Here, our method meaningfully outperforms HEVC in SSIM metrics while further reducing the gap in the PSNR. It is worth noting that for quality assessment, the SSIM metric is more reliable than PSNR.

As shown in Table 1, the compression time of our proposed method is more than 100 times faster than that of HEVC, on the same computational hardware. This is because of our more efficient compression pipeline, which is just a JPEG algorithm on a fraction of the LF ( $1/49$  in our case with 49 views). The HEVC algorithm processes all of the views.

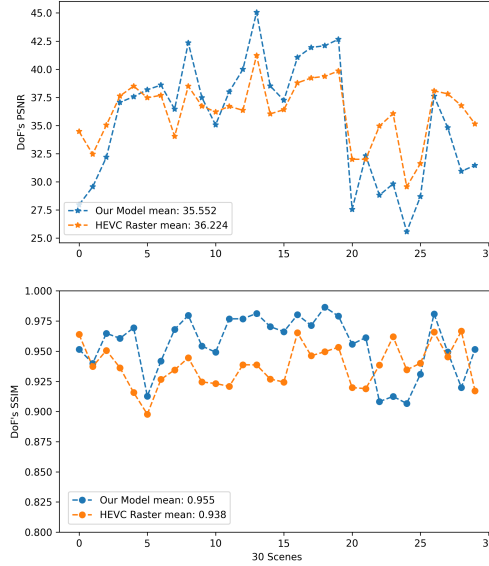


Figure 5: The DoF images extracted from ground truth LFs and the reconstructed LFs are compared using SSIM and PSNR metrics. The top plot is representing PSNR and the bottom one is showing SSIM for each LF in the 30 scenes.

Method	CUDA	Comp time (s)
HEVC	No	43.53
JPEG-Hance + Depth-Net	No	<b>0.42</b>

Table 1: The time takes to compress all 30 LFs in the 30 scenes data set using our method and the HEVC. We can see an speed up of more than 102 times.

For decompression, our method is 18 times faster than HEVC; see Table 2. To give a fair comparison, we used the NVIDIA optimized HEVC codec using the GPU’s video decoder. So on the same hardware, this will be the fastest implementation of HEVC.

Overall, these results indicate that our model is suitable for compressing light field videos with high angular resolution. This is because it can be decompressed in near real time inside the GPU without the barrier of transferring high volumes of data from host to GPU. The bandwidth used from host to GPU is equal to the size of only the center view of the LF.

## 5 Conclusions

We have designed a machine-learning assisted LF compression technique. It contains two sequential CNNs (JPEG-Hance and Depth-Net). We showed that there is enough information in a highly compressed LF center view to estimate a depth-map for LF and use it to reconstruct the whole LF. Also, compression and decompression are faster with our method. We have used the public *Flowers* and *30 Scenes* data sets to conduct our experiment and also to evaluate our model. We have achieved more than 100 times speedup during compression and about 18 times faster reconstruction compared to using HEVC on LF pseudo sequences. Comparing to HEVC, the reconstructed LFs using our method

Method	CUDA	Rec time (s)
HEVC	yes	0.399
JPEG-Hance + Depth-Net	yes	<b>0.022</b>

Table 2: The reconstruction time on all LFs from the 30 scenes data set by our method and HEVC. We can see that our method is 18 times faster in decompressing.



have superior MSSIMs, and they have comparable MPSNRs. For future work, we will try to add some other views to improve the quality of reconstruction. The added views possibly will be more compressed than the center view. We will also explore options to enhance the MPSNR. We are looking forward to deploying our method on an actual LF video to explore the achieved compression ratio and streaming capabilities.

## References

- [1] D. Liu, L. Wang, L. Li, Zhiwei Xiong, Feng Wu, and Wenjun Zeng. Pseudo-sequence-based light field image compression. In *2016 IEEE International Conference on Multimedia Expo Workshops (ICMEW)*, pages 1–4, 2016.
- [2] Z. Zhao, S. Wang, C. Jia, X. Zhang, S. Ma, and J. Yang. Light field image compression based on deep learning. In *2018 IEEE International Conference on Multimedia and Expo (ICME)*, pages 1–6, 2018.
- [3] A. Levin and F. Durand. Linear view synthesis using a dimensionality gap light field prior. In *2010 IEEE Computer Society Conference on Computer Vision and Pattern Recognition*, pages 1831–1838, 2010.
- [4] T. E. Bishop and P. Favaro. The light field camera: Extended depth of field, aliasing, and superresolution. *IEEE Transactions on Pattern Analysis and Machine Intelligence*, 34(5):972–986, 2012.
- [5] John Flynn, Ivan Neulander, James Philbin, and Noah Snavely. Deepstereo: Learning to predict new views from the world’s imagery. In *Proceedings of the IEEE Conference on Computer Vision and Pattern Recognition (CVPR)*, June 2016.
- [6] Nima Khademi Kalantari, Ting-Chun Wang, and Ravi Ramamoorthi. Learning-based view synthesis for light field cameras. *ACM Trans. Graph.*, 35(6), November 2016.
- [7] Henry Wing Fung Yeung, Junhui Hou, Jie Chen, Yuk Ying Chung, and Xiaoming Chen. Fast light field reconstruction with deep coarse-to-fine modeling of spatial-angular clues. In *The European Conference on Computer Vision (ECCV)*, September 2018.
- [8] Pratul P. Srinivasan, Tongzhou Wang, Ashwin Sreelal, Ravi Ramamoorthi, and Ren Ng. Learning to synthesize a 4d rgbd light field from a single image. In *The IEEE International Conference on Computer Vision (ICCV)*, Oct 2017.
- [9] Inchang Choi, Orazio Gallo, Alejandro Troccoli, Min H. Kim, and Jan Kautz. Extreme view synthesis. In *The IEEE International Conference on Computer Vision (ICCV)*, October 2019.
- [10] Ben Mildenhall, Pratul P. Srinivasan, Rodrigo Ortiz-Cayon, Nima Khademi Kalantari, Ravi Ramamoorthi, Ren Ng, and Abhishek Kar. Local light field fusion: Practical view synthesis with prescriptive sampling guidelines. *ACM Trans. Graph.*, 38(4), July 2019.
- [11] Wenhui Zhou, Gaomin Liu, Jiangwei Shi, Hua Zhang, and Guojun Dai. Depth-guided view synthesis for light field reconstruction from a single image. *Image and Vision Computing*, 95:103874, 2020.
- [12] Zexi Hu, Yuk Ying Chung, Wanli Ouyang, Xiaoming Chen, and Zhibo Chen. Light field reconstruction using hierarchical features fusion. *Expert Systems with Applications*, 151:113394, 2020.
- [13] Cristian Perra. Lossless plenoptic image compression using adaptive block differential prediction. In *2015 IEEE International Conference on Acoustics, Speech and Signal Processing (ICASSP)*, pages 1231–1234. IEEE, 2015.
- [14] Petri Helin, Pekka Astola, Bhaskar Rao, and Ioan Tabus. Sparse modelling and predictive coding of subaperture images for lossless plenoptic image compression. In *2016 3DTV-Conference: The True Vision-Capture, Transmission and Display of 3D Video (3DTV-CON)*, pages 1–4. IEEE, 2016.
- [15] C. Conti, P. Nunes, and L. D. Soares. Hvc-based light field image coding with bi-predicted self-similarity compensation. In *2016 IEEE International Conference on Multimedia Expo Workshops (ICMEW)*, pages 1–4, 2016.
- [16] Y. Li, R. Olsson, and M. Sjöström. Compression of unfocused plenoptic images using a displacement intra prediction. In *2016 IEEE International Conference on Multimedia Expo Workshops (ICMEW)*, pages 1–4, 2016.
- [17] M. Le Pendu X. Jiang and C. Guillemot. Light field compression using depth image based view synthesis. In *2017 IEEE International Conference on Multimedia Expo Workshops (ICMEW)*, pages 19–24, 2016.
- [18] E. Dib, M. L. Pendu, and C. Guillemot. Light field compression using fourier disparity layers. In *2019 IEEE International Conference on Image Processing (ICIP)*, pages 3751–3755, 2019.
- [19] I. Tabus, P. Helin, and P. Astola. Lossy compression of lenslet images from plenoptic cameras combining sparse predictive coding and jpeg 2000. In *2017 IEEE International Conference on Image Processing (ICIP)*, pages 4567–4571, 2017.
- [20] X. Jiang, M. Le Pendu, R. A. Farrugia, and C. Guillemot. Light field compression with homography-based low-rank approximation. *IEEE Journal of Selected Topics in Signal Processing*, 11(7):1132–1145, 2017.
- [21] J. Zhao, P. An, X. Huang, L. Shan, and R. Ma. Light field image sparse coding via cnn-based epi super-resolution. In *2018 IEEE Visual Communications and Image Processing (VCIP)*, pages 1–4, 2018.
- [22] B. Wang, Q. Peng, E. Wang, K. Han, and W. Xiang. Region-of-interest compression and view synthesis for light field video streaming. *IEEE Access*, 7:41183–41192, 2019.

- [23] Chao Dong, Yubin Deng, Chen Change Loy, and Xiaoou Tang. Compression artifacts reduction by a deep convolutional network. In *The IEEE International Conference on Computer Vision (ICCV)*, December 2015.
- [24] Jun Guo and Hongyang Chao. Building dual-domain representations for compression artifacts reduction. In Bastian Leibe, Jiri Matas, Nicu Sebe, and Max Welling, editors, *Computer Vision – ECCV 2016*, pages 628–644, Cham, 2016. Springer International Publishing.
- [25] Zhangyang Wang, Ding Liu, Shiyu Chang, Qing Ling, Yingzhen Yang, and Thomas S. Huang. D3: Deep dual-domain based fast restoration of jpeg-compressed images. In *The IEEE Conference on Computer Vision and Pattern Recognition (CVPR)*, June 2016.
- [26] Xiaojiao Mao, Chunhua Shen, and Yu-Bin Yang. Image restoration using very deep convolutional encoder-decoder networks with symmetric skip connections. In D. D. Lee, M. Sugiyama, U. V. Luxburg, I. Guyon, and R. Garnett, editors, *Advances in Neural Information Processing Systems 29*, pages 2802–2810. Curran Associates, Inc., 2016.
- [27] L. Cavigelli, P. Hager, and L. Benini. Cas-cnn: A deep convolutional neural network for image compression artifact suppression. In *2017 International Joint Conference on Neural Networks (IJCNN)*, pages 752–759, 2017.
- [28] Baochang Zhang, Jiaxin Gu, Chen Chen, Jungong Han, Xiangbo Su, Xianbin Cao, and Jianzhuang Liu. One-two-one networks for compression artifacts reduction in remote sensing. *ISPRS Journal of Photogrammetry and Remote Sensing*, 145:184 – 196, 2018. Deep Learning RS Data.
- [29] X. Zhang, W. Yang, Y. Hu, and J. Liu. Dmccn: Dual-domain multi-scale convolutional neural network for compression artifacts removal. In *2018 25th IEEE International Conference on Image Processing (ICIP)*, pages 390–394, 2018.
- [30] Z. Jin, M. Z. Iqbal, W. Zou, X. Li, and E. Steinbach. Dual-stream multi-path recursive residual network for jpeg image compression artifacts reduction. *IEEE Transactions on Circuits and Systems for Video Technology*, pages 1–1, 2020.
- [31] Zhou Wang, A. C. Bovik, H. R. Sheikh, and E. P. Simoncelli. Image quality assessment: from error visibility to structural similarity. *IEEE Transactions on Image Processing*, 13(4):600–612, 2004.
- [32] Clement Godard, Oisín Mac Aodha, and Gabriel J. Brostow. Unsupervised monocular depth estimation with left-right consistency. In *Proceedings of the IEEE Conference on Computer Vision and Pattern Recognition (CVPR)*, July 2017.
- [33] Yang Wang, Yi Yang, Zhenheng Yang, Liang Zhao, Peng Wang, and Wei Xu. Occlusion aware unsupervised learning of optical flow. In *Proceedings of the IEEE Conference on Computer Vision and Pattern Recognition (CVPR)*, June 2018.
- [34] Zhichao Yin and Jianping Shi. Geonet: Unsupervised learning of dense depth, optical flow and camera pose. In *Proceedings of the IEEE Conference on Computer Vision and Pattern Recognition (CVPR)*, June 2018.